

4-dimensional Printing of Multi-material, Multi-shape Changing Shape Memory Polymer Composites

MANIKANDAN.N*¹ AND RAJESH.P.K¹

¹Department of Automobile Engineering, PSG College of Technology,
Coimbatore -641004, India.

ABSTRACT

In this research, a new method to fabricate multi-material, multi-shape changing polymer composites is proposed. The method aims to reduce the number of thermomechanical programming steps involved in achieving shape change in a shape memory polymer (SMP) composite structure by including the programming steps directly into the printing process. After a single step of mechanical deformation and thermal loading, the SMP fibers can be activated sequentially to control the shape change. Composite strip samples were fabricated using a Stratasys Objet 260 multimaterial printer. Two polymer inks VeroPureWhite and Agilus30 were used as primary materials. The composite strip consists of fiber layers made of digital materials (DM) namely RGD8525 and FLX9895 which are embedded in an elastomer matrix material Agilus30. The glass transition temperature of the sample materials was measured using the DMA fixture of Anton Paar MCR 102 rheometer in film tension mode and the values for the matrix, fiber 1 and fiber 2 are 4°C, 52°C and 32°C respectively. Fiber 1 and fiber 2 materials have distinct T_g values enabling the possibility of multiple shape memory effect. Uniaxial tensile tests were performed using a universal tensile testing machine, ZwickRoell Z010 to understand the stress-strain behavior of the sample materials. At 25°C, fiber 1 exhibits elastoplastic behavior and as the temperature is increased to 60°C the behavior changes to linear elastic. The Young's modulus of the matrix material is considerably lower than the two fiber materials indicating that the fiber materials can induce shape change effect in the composite strip. The designed composite structure was able to display shape change in two different modes: bridge and cantilever. The shape change responses were achieved at 9 seconds and 7 seconds in the bridge and cantilever modes respectively which indicated that composite structures can be actuated sequentially. With the key advantages of multiple shape changes and an easy fabrication process, the direct

4D printing of shape memory polymer composite structures display vast potential in 4D printing applications including medical, automobile and aerospace applications.

KEYWORDS: *4D printing, Inkjet printing, Shape memory polymer, Composite, Multi-shape change.*

1. INTRODUCTION

The 3D printing, also known as additive manufacturing, allows complex structures to be manufactured from a three-dimensional computer model. The 3D printing process has several advantages such as design freedom to produce complex structures, scalability, rapid prototyping, product customization, and raw material saving^[1]. However, the process also suffers from disadvantages such as need for support structures while printing overhangs, slow printing times and difficulty in printing hollow/slender structures. Meanwhile, 4D printing has emerged as a manufacturing method in which a 3D structure is printed and transformed into a complex assembly when subjected to external stimuli such as light, temperature, solvents, humidity, magnetic field, etc.,^[2]. Skylar Tibbitts originally proposed the notion of 4D printing at a TED conference in 2013, where the shape change behaviour of a static structure over time was demonstrated^[3]. The materials used in 4D printing are referred as Stimulus Responsive Materials (SRMs) as the printed structures change shape or a property when exposed to an external stimulus. The different categories of SRMs used in 4D printing are Shape Memory Alloy (SMA), Shape Memory Polymer (SMP), Shape Memory Ceramic (SMC), Shape Memory Gel (SMG) and Shape Memory Hybrid (SMH)^[2]. SMPs have gained favor among SRMs due to their biocompatibility, low cost, high strain recovery

and low density^[4]. The advantages of 4D printing with SMPs include a reasonably rigid construction and a comparatively fast actuation speed, both of which are orders of magnitude better than those produced with other printed SRMs^[5]. From the product manufacturing stance, 4D printing displays the potential to produce complex 3D structures from 1D^[6] or 2D^[7-9] primitive structures. This has the potential to save both raw resources and production time, as well as provide additional programmed functionality.

In general, 4D printing with SMPs entails the following steps: processing by 3D printing, thermomechanical programming and deployment/actuation. The thermomechanical programming is highly significant determining the overall shape recovery performance of the printed structure. The thermomechanical programming process includes heating, mechanical loading, cooling and removal of load. This process often requires fixtures to perform mechanical loading and unloading. The as-printed structures are generally stress free and are in a low energy level. External stress is applied directly to the printed SMP structure via mechanical loading and thermomechanical programming is performed to achieve shape recovery^[10-14]. Stimulation using external loading reduces the shape recovery capability and makes the shape recovery unstable^[15].

A SMP requires at least one glass transition temperature (T_g) to achieve shape memory

effect between two different shapes. It is preferable to create SMPs or composites that can switch between several forms in a predictable manner. Two or more transition temperatures are required to create multiple shape changes. As an example, Xie, Xiao^[16] and Luo and Mather^[17] demonstrated triple shape memory effects in polymers with different glass transition temperatures and melt-transition points. Also multiple shape changing effects in SMPs were demonstrated using Digital SMP materials by Mao, Yu^[9], Yu, Ritchie^[8] and Yu, Dunn^[18]. Digital SMP materials are obtained by coalescing and printing polymers with different properties to obtain 3D structures with desirable thermomechanical properties by design.

A new method is proposed in this research, wherein a multi-material SMP composite strip is fabricated with the programming steps included directly into the printing process. The proposed method aims to induce internal stress directly into the component during the 3D printing process by controlling the photopolymerization effectively. Once printed, the printed components can be directly heated/cooled to perform multiple shape changes thereby reducing the number of thermomechanical programming steps. The fabricated SMP structure can be activated to the desired shape with a single step of heating. The proposed design concept is illustrated in Figure 1.

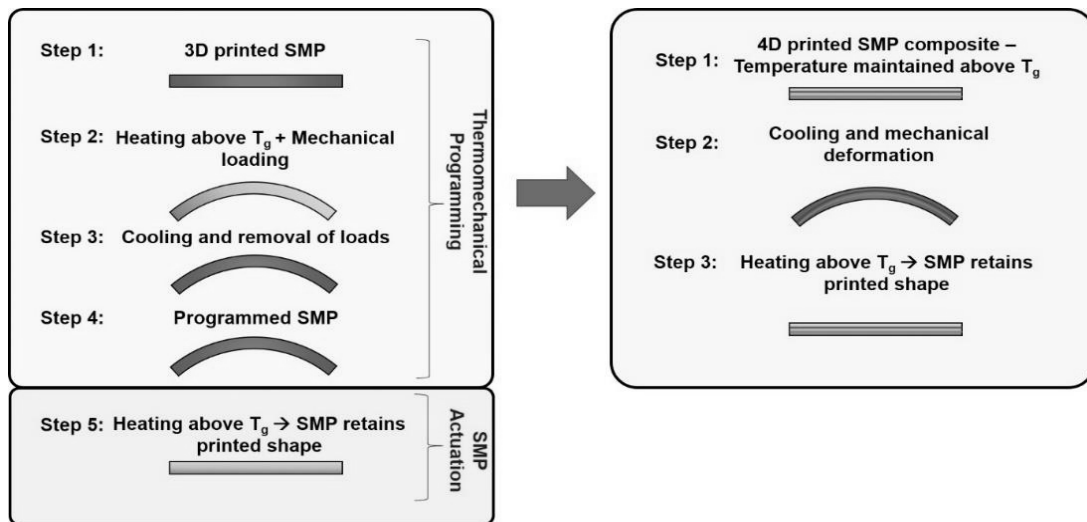


Figure 1. Design concept for direct 4D printing of SMP composites.

2. MATERIALS AND METHODS

2.1 Materials and Composite Design

The fabricated composite strips consist of two digital materials (Fiber 1: RGD8525 and Fiber 2: FLX9895)

embedded as fibers in an elastomer matrix (Matrix: Agilus30). The digital materials are created by mixing a primary material (VeroPureWhite) and a secondary material (Agilus30). VeroPureWhite is a rigid plastic and TangoPlus is an elastomer at room temperature. Ding, Yuan^[19] studied the effect of layer printing time (LPT)

versus internal compressive strain (CS), layer printing time versus and curvature (ρ) and also volume fraction (VF) of elastomer versus curvature while inkjet 4D printing of elastomers. The authors showed that the internal compressive strain and curvature increase with increase in the layer printing time and elastomer fraction respectively during inkjet printing. Polynomial interpolation was used to derive the relationship between the factors as shown in Equations (1) – (3).

$$\rho = -3E^{-9}VF^4 + 3E^{-7}VF^3 + 9E^{-6}VF^2 - 0.0003VF + 0.0045 \quad (1)$$

$$CS (\%) = -0.0004LPT^2 + 0.0596LPT + 0.5685 \quad (2)$$

$$\rho = -8E^{-6}LPT^2 + 0.0012LPT + 0.0038 \quad (3)$$

Based on Equations (1)-(3), composite strip samples were printed with a layer printing time of 50 seconds to achieve a strain recovery of ~2.5% and designed to retain shape up to a curvature of 50 mm^{-1} . The composite strip is 50 mm long, 5 mm wide, and 2 mm thick, with the fiber dimensions of $0.30 \text{ mm} \times 0.30 \text{ mm}$ and the fibers are uniformly spaced by 0.3 mm from each other accounting to eight fibers each of Fiber 1 and Fiber 2. The fibers are placed at 0.35 mm from the top and bottom of the matrix to maintain fiber volume fraction of 15%. The dimensions and a sample of the 4D printed composite strip is shown in Figure 2.

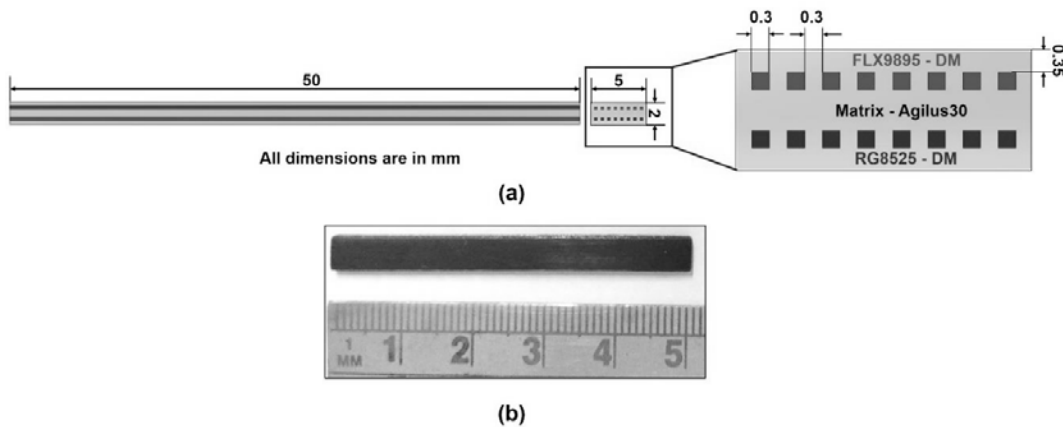


Figure 2. Design of composite strip (a) Dimensions of the composite strip; (b) Top view of the 4D printed composite strip.

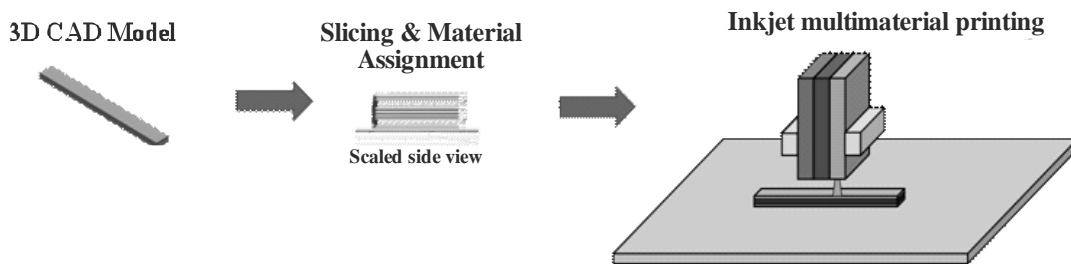


Figure 3. Schematic showing the process of inkjet multimaterial printing

The composite strips were fabricated using a Stratasys Objet 260 Connex multimaterial printer. The printer has the ability to print different materials layer by layer as it consists of multiple printheads that hold ink materials of various rheological properties. The schematic of the multimaterial printing process is shown in Figure 3. The 3D model was created for the required dimensions in a commercially available CAD package and converted in to STL format. The file is then imported in to GrabCAD print (Stratasys slicing software for inkjet printers) and different materials were assigned for the matrix and the fiber components of the composite strip. Once the required printing parameters were set, the model was loaded into the printer for printing.

2.2 Dynamic Mechanical Analysis (DMA)

The glass transition temperature (T_g) of the materials were measured using the DMA fixture of Anton Paar MCR102 rheometer in film tension mode. The 20 mm x 10 mm x 1 mm sample materials were heated to 80°C and cooled down to -40°C at a rate of 2°C/min^[20]. The temperature range at which the sample changes to a glassy state from a solid state was chosen for the analysis. The samples were preloaded with a controlled strain ramp of 0.1%/s. The variation of storage modulus and $\tan \delta$ with temperature for the selected materials is shown in Figure 4. The glass transition temperatures (T_g) for the sample materials is the temperature at which $\tan \delta$ reaches the maximum value as shown in Figure 4(b).

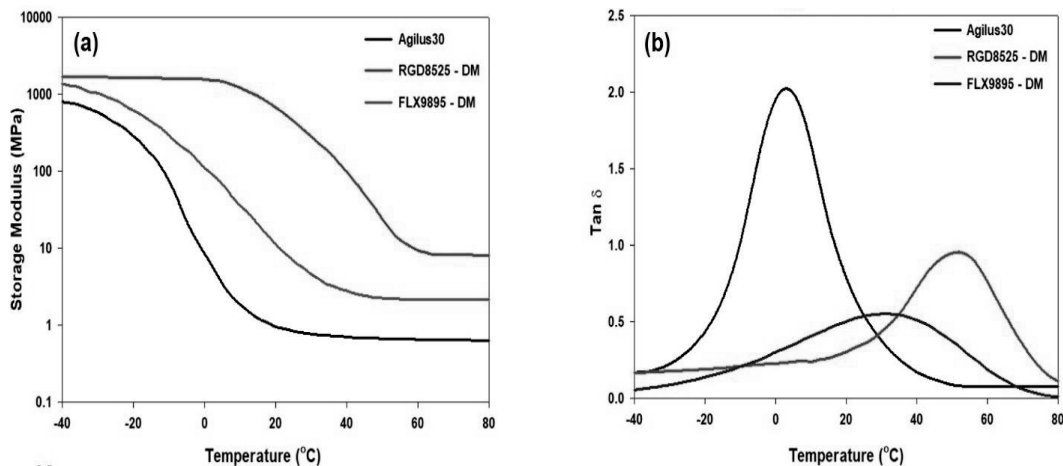


Figure 4. Results of DMA (a) Variation of storage modulus with temperature; (b) Variation of $\tan \delta$ with temperature.

2.3 Tensile Testing

The uniaxial tensile test was performed to understand the mechanical behavior of the sample materials. The sample sizes following ASTM D638-14 test standard were tested using a universal tensile testing machine (ZwickRoell Z010) with 2 mm/min strain loading until fracture. For the tensile measurement at 60°C for Fiber 1 (RGD8525), the sample was heated to the required temperature inside a thermal chamber and the stress-strain measurements were made.

Figure 5 represents the stress-strain behavior the sample materials. The stress-strain behavior of the sample materials is highly temperature dependent which is consistent with the existing polymer characterization studies^[21-23]. At 25°C, Fiber 1 exhibits elastoplastic behavior and as the temperature is increased to 60°C the behavior changes to linear elastic. The Young's modulus of the matrix material is considerably lower than the two fiber materials indicating that the fiber materials can induce shape change effect in the composite strip.

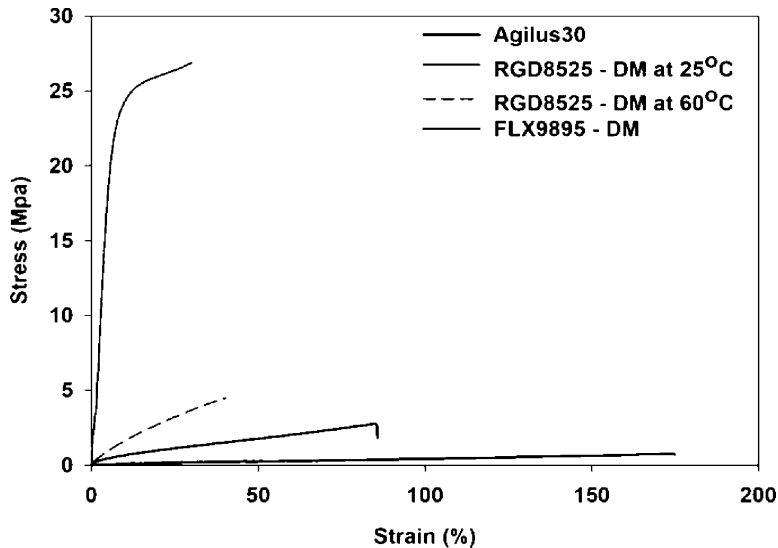


Figure 5. Stress-Strain behavior of the sample materials.

As the composite structure can undergo large deformations during the shape recovery process it is considered important to study the effect of temperature on the failure strain of the sample materials. Since the matrix material Agilus 30 is an elastomer it has the highest failure strain of ~175%. Since the fiber materials RGD8525 and FLX9895 are a mixture of VeroPureWhite and Agilus30, the fracture strain highly depends on the ratio of the two base

materials. The fracture strain of Fiber 1 (RGD8525) is ~30% at room temperature and increases to ~40% at 60°C. The fracture strain of Fiber 2 (FLX9895) is ~85% at room temperature. The fracture strain of the fibers indicates the shape memory effect can be obtained within strain values up to 40%. The viscoelastic parameters identified from the DMA and tensile tests are shown in Table 1.

TABLE 1. Viscoelastic parameters of the sample materials identified from the DMA and tensile tests

Material	T _g (°C)	Young's Modulus (MPa)	Fracture Strain (%)
Matrix (Agilus30)	4	0.98	174.52
Fiber 1 (RGD8525)	52	448.34 @ 25°C	29.95
		10.80 @ 60°C	40.12
Fiber 2 (FLX9895)	32	13.03	84.96

It is observed from Table 1 that the glass transition temperature of the fiber materials varies between 32°C to 52°C which indicates the shape memory effect

can be obtained in the same temperature range. Because the matrix materials' T_g is lower than room temperature, it displays elastic stress-strain behavior

with a significant failure strain and poor tensile strength. Fiber 1 and Fiber 2 materials have distinct Tg values of 52°C and 32°C enabling the possibility of multiple shape memory effect.

2.4 Thermomechanical Programming and Shape Memory Behavior

The temperature during printing of the composite strip was maintained at 70°C which is above the Tg of the sample materials used. This process ensures the reduction of the thermomechanical programming needed to achieve shape memory effect. A small channel shaped fixture was 3D printed using PLA to mechanically deform the composite strip. The composite strip was deformed to a curved shape with an initial curvature of 50 mm⁻¹ which is below the maximum allowable strain for the composite strip. Once the

composite strip was fixed, the fixture is held inside a glass container filled with clear water. The temperature of the water inside the container was raised from a room temperature of 28°C to a temperature above Tg of the sample materials. The composite strip held a secondary temporary shape when the temperature is maintained at ~40°C which is above the Tg of Fiber 2 and was able to display complete shape change to the initial printed shape at ~70°C. It was observed that the total time for shape recovery is 9 seconds indicating the fast shape change capability of the composite strip. The repeatability of the shape change was confirmed with a total of three samples of the composite strip and the shape change effect observed is shown in Figure 6. The variation in curvature of the composite strip at different temperatures is shown in Figure 7.

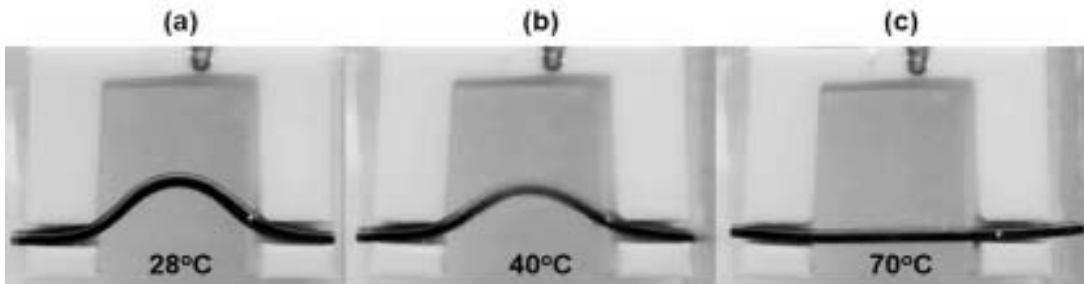


Figure 6. Multi-shape change behavior of the direct 4D printed composite strip (a) deformed shape at 28°C; (b) temporary shape at 40°C; and (c) initial printed shape at 70°C

To validate the shape recovery capability, one sample of the composite strip was deformed into cantilever mode. The temperature of the water inside the container was raised similar to the previous experiment. The composite strip was able to hold a temporary shape at ~40°C and display complete shape change to the initial printed shape at ~70°C. The complete shape change was achieved in 7 seconds. The shape change behavior of the composite strip in cantilever mode is shown in Figure 8.

2.5 Shape Recovery Performance

The two important parameters reflecting the shape memory performance of SMPs are Shape Fixity Ratio

(*Rf*) and Shape Recovery Ratio (*Rr*). *Rf* shows the capability of the SMP to fix the mechanical deformation in the thermomechanical process and *Rr* shows the capability of the material to recover to its original shape. The values of *Rf* and *Rr* are determined by Equations (4) and (5).

where, ϵ_{load} – strain above Tg, ϵ_{unload} – strain measured after cooling below Tg and removal of mechanical loading and ϵ_{final} – strain measured when the printed parts have recovered to their original shape. Using the DMA fixture of Anton Paar MCR102 rheometer

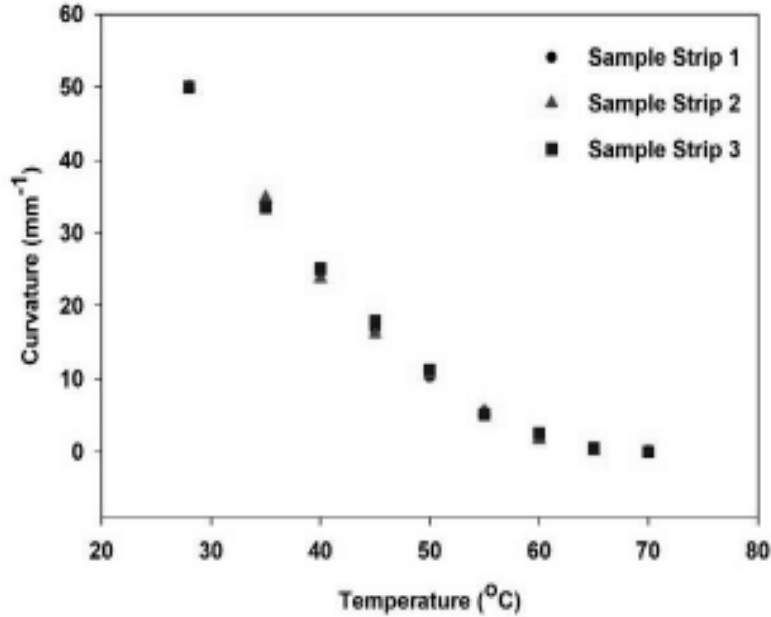


Figure 7. Variation in curvature of the sample composite strips with temperature

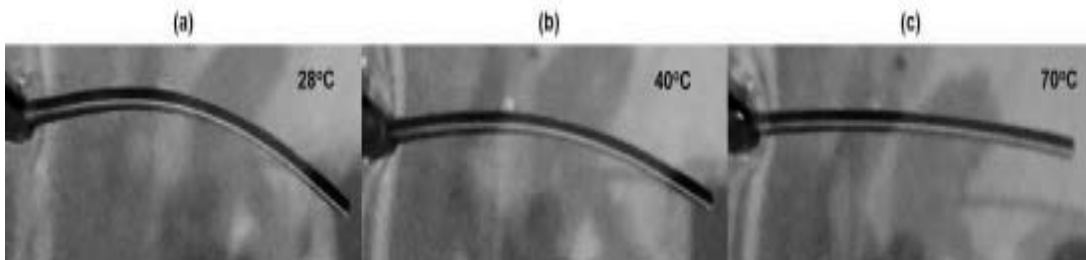


Figure 8. Multi-shape change behavior of the direct 4D printed composite strip in cantilever mode (a) deformed shape at 28°C; (b) temporary shape at 40°C; and (c) initial printed shape at 70°C.

in film tension mode, the shape fixity and shape recovery ratios are measured by the following steps: (1) Heating the samples to a temperature 30°C above T_g at a rate of 2°C/min; (2) deformation of the samples with a force of 0.1 N/min and strain up to 2.5%; (c) cooling the samples to room temperature without removing the load; (d) shape fixing by removing the applied load and (e) shape recovery where the

samples are reheated to 10°C above T_g . The final strain values calculated at each step was

$$R_f = \frac{\epsilon_{unload}}{\epsilon_{load}} \times 100\% \quad (4)$$

$$R_r = \frac{\epsilon_{unload} - \epsilon_{final}}{\epsilon_{unload}} \times 100\% \quad (5)$$

used to calculate the shape recovery and fixity values as shown in Figure 9. The samples were able to display an average shape fixity ratio of 94.4% and shape recovery ratio of 99.4%.

3. CONCLUSION

Direct 4D printing of a multi-material, multi-shape change SMP composite was demonstrated in

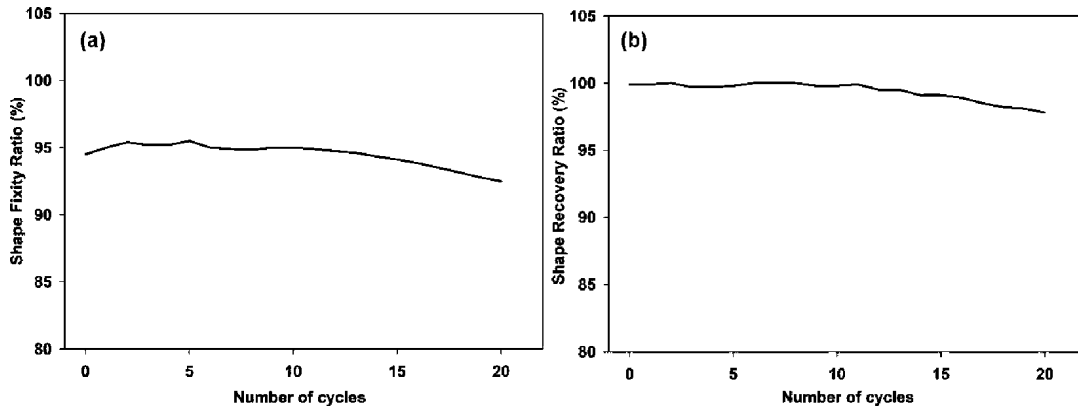


Figure 9. Shape recovery performance of the printed samples (a) Shape Fixity Ratio; (b) Shape Recovery Ratio.

this research. The direct 4D printing technology will find applications in the fabrication of biomedical devices, wearable devices and artificial muscles. The application of this research is in the fabrication of complex structural elements capable of conveying flexibility achieved through the combination of material, process design and geometrical parameters. The main concept is to print samples in flat, layered configurations that are easy to design and print in terms of both printing time and material waste because no support material is required. They are then used to create various 3D permanent forms via a simple heating phase. 2D flat sheets can be purposefully transformed into a 3D structure using a required smart material. Direct 4D printing may be used to incorporate functional

devices as a platform technology. A flat transformable sheet, for example, can be produced. The flat sheet may then be used to build conductive circuits and electronic components like as batteries, sensors, and actuators; its flat shape facilitates these integration activities. The flat construction might then be heated to form a desired 3D structure with built-in electrical capabilities. This new design and printing approach enables multi-material printed structures to achieve shape memory effect with a single step reducing the thermomechanical programming steps from four to one. The design concept also facilitates the fabrication of structures that can change into multiple configurations rather than a single configuration which opens new possibilities to integrate functional devices. The fabricated composite strips were able to display

multi-shape change effects in two different modes: bridge and cantilever. The shape change behavior was also repeatable and faster response was achieved in the cantilever mode at 7 seconds. The shape fixity and recovery ratios of the samples were 94.4% and 99.4% respectively indicating reproducibility and predictability of the shape recovery performance. The combination of the shape changing experiment reveals that composite structures can be 4D printed using SMP materials in a reproducible and predicable means. Evidently, the proposed approach can pave way for the effective manufacturing of complex 3D and deployable self-assembly structures via 4D printing of SMPs without the need for support materials and thermomechanical programming.

REFERENCES

1. D. Raviv, W.Zhao, C.McKnelly, A.Papadopoulou, A.Kadambi, B.Shi, S.Hirsch, D.Dikovsky, M.Zyracki, C.Olguin, R.Raskar and S.Tibbits, *Sci Rep.* 4, (2014), 7422.
2. J. Choi, O.C. Kwon, W. Jo, H.J. Lee and M.W. Moon, *3D Print. Addit. Manuf.* 2(4), (2015), 159.
3. K. Yu, A. Ritchie, Y. Mao, M.L. Dunn and H.J. Qi, *Procedia IUTAM.* 12, (2015), 193.
4. K. Yu, M.L. Dunn and H.J. Qi, *Extreme Mech. Lett.* 4, (2015), 9.
5. M. Bodaghi, A.R. Damanpack and W.H. Liao, *Smart Mater. Struct.* 25(10), (2016), 105034.
6. N. Lagakos, J. Jarzynski, J.H. Cole and J.A. Bucaro, *J. Appl. Phys.* 59(12), (1986), 4017.
7. Q. Ge, C.K. Dunn, H.J. Qi and M.L. Dunn, *Smart Mater. Struct.* 23(9), (2014) 94007.
8. Q. Ge, H.J. Qi and M.L. Dunn, *Appl. Phys. Lett.* 103(13), (2013), 131901.
9. S.A.M. Tofail, E.P. Koumoulos, A. Bandyopadhyay, S. Bose, L. O'Donoghue and C. Charitidis, *Mat. Today.* 21 (1), (2018), 22.
10. S. Deng, M. Hou and L. Ye, *Polym. Test.* 26(6), (2007), 803.
11. S. Joshi, K. Rawat, C. Karunakaran, V. Rajamohan, A.T. Mathew, K. Koziol, V. Kumar Thakur and A.S.S. Balan, *Mater. Today* 18, (2020), 100490.
12. S. Tibbits, C. McKnelly, C. Olguin, D. Divkovsky and S. Hirsch, In Proceedings of the 34th Annual Conference of the Association for Computer Aided Design in Architecture (2014) pp 539-548.
13. S. Tibbits, The emergence of 4D printing, *TED*, (2013).
14. T.A. Campbell, S. Tibbits and B. Garrett, *Sci. Am.* 311(5), (2014), 60.
15. T. Xie, X. Xiao and Y.T. Cheng, *Macromol. Rapid Commun.* 30(21), (2009), 1823.
16. X. Luo and P.T. Mather, *Adv. Funct. Mater.* 20(16), (2010), 2649.
17. Y.S. Alshebly, M. Nafea, M.S. Mohamed Ali and H.A.F. Almurib, *Eur. Polym. J.* 159 (2021), 11078.
18. Y. Li, F. Zhang, Y. Liu and J. Leng, *Sci. China: Technol. Sci.* 63(4), (2020), 545.
19. Y. Liu, K. Gall, M.L. Dunn, A.R. Greenberg and J. Diani, *Int. J. Plast.* 22(2), (2006), 279.
20. Y. Mao, K. Yu, M.S. Isakov, J. Wu, M.L. Dunn and H.J. Qi, *Sci Rep.* 5, (2015), 1.
21. Z. Ding, O. Weeger, H.J. Qi and M.L. Dunn, *Mater. Des.* 137, (2018), 256.
22. Z. Ding, C. Yuan, X. Peng, T. Wang, H.J. Qi and M. L. Dunn, *Sci. Adv.* 3(4), (2007), 2890.
23. Z. Jin, K.P. Pramoda, G. Xu and S.H. Goh, *Chem. Phys. Lett.* 337(3), (2001), 43.

Received: 01-09-2021

Accepted: 19-11-2021